Science Advances
AAAS

advances.sciencemag.org/cgi/content/full/3/3/e1602462/DC1

Supplementary Materials for

Programmable and coherent crystallization of semiconductors

Liyang Yu, Muhammad R. Niazi, Guy O. Ngongang Ndjawa, Ruipeng Li, Ahmad R. Kirmani, Rahim Munir, Ahmed H. Balawi, Frédéric Laquai, Aram Amassian

Published 3 March 2017, *Sci. Adv.* **3**, e1602462 (2017)
DOI: 10.1126/sciadv.1602462

The PDF file includes:

Other Supplementary Material for this manuscript includes the following:
(available at advances.sciencemag.org/cgi/content/full/3/3/e1602462/DC1)

- movie S1 (format). Conventional crystallization of a TES ADT film proceeding stochastically and incoherently.

- movie S2 (format). Linear programmed crystallization of TES ADT proceeding simultaneously and coherently from horizontal seeding lines.
- movie S3 (format). Periodic dot array crystallization of TES ADT proceeding simultaneously and coherently from an array of imprinted seed dots.
- movie S4 (format). Square programmed crystallization of TES ADT proceeding simultaneously and coherently from horizontal and vertical seeding lines.
- movie S5 (format). Square and rectangular programmed crystallization of TES ADT proceeding simultaneously and coherently from horizontal and vertical seeding lines.

Supplementary Materials

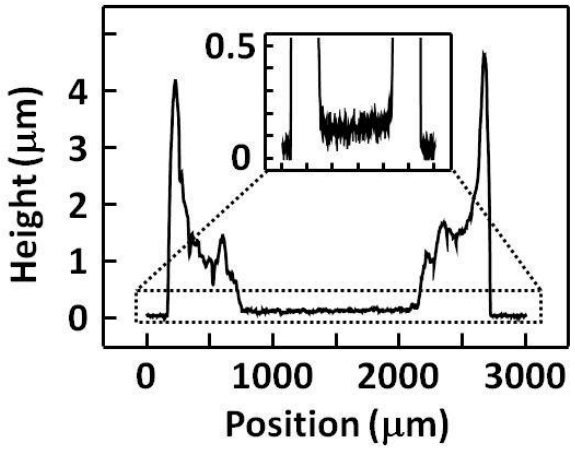

fig. S1. Height profile of the solidified droplet of TES ADT. The inset shows the height of the central section of the solidified droplet.

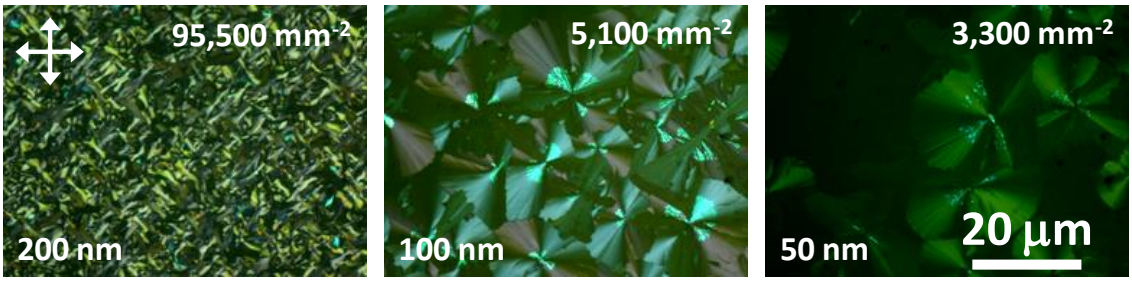

fig. S2. Polarized optical micrographs of MoO_x thin films with different thicknesses. The nucleation density is obtained by counting the spherulites in a representative area of the film and is marked in the top right corner.

Discussion: Thickness-dependent nucleation density observed in commodity polymers has been attributed to spatial confinement effects, as the size of polymer nuclei and the film thickness were found to be very close (*41*). However, the size of critical nuclei in inorganic systems or small molecule systems is comparatively minuscule, typically forming small nanoclusters made up of a few atoms or molecules, and should therefore not be subject to confinement effects in comparatively thick films (10s – 100s nm). Such confinement effects are likely to be the reason for the 2D powder textured microstructure observed in the thin films investigated in this study. The formation of large domains (>> *d*) with textured microstructure is attributed to the selective growth of a subset of bulk nuclei whose fast growth directions are in the plane of the thin film, i.e., parallel to the substrate. Hence, a subset of the randomly oriented nanoscopic nuclei are free to propagate laterally up to macroscopic scales. These nuclei appear to seed the subsequent conversion of the entire film forming textured structures.

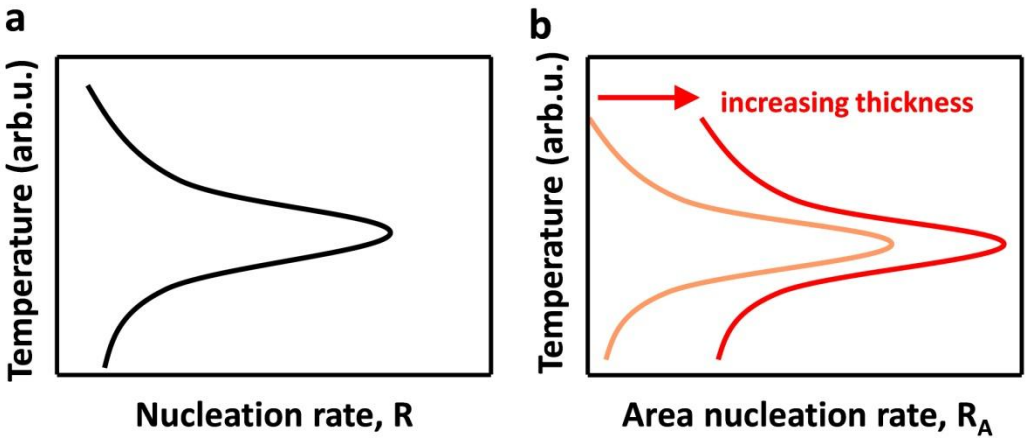

fig. S3. Illustrative plots of the volumetric and areal nucleation rates with respect to temperature. (A) Illustrative plot of the volumetric nucleation rates *R* with respect to temperature on the ordinate. (B) Illustrative plots of the areal nucleation rates R_A with respect to temperature on the ordinate where the influence of thickness is taken in consideration.

Discussion: Nucleation events occur when the Gibbs free energy of nucleus formation (ΔG^*) is overcome and the diffusion of atoms or molecules, as defined by a diffusion activation energy (Q), is favorable. R can be mathematically expressed as (*42*)

$$R \equiv \frac{N}{\Delta t \Delta V} = K\, exp\left(-\frac{\Delta G^*}{kT}\right)\, exp\left(-\frac{Q}{kT}\right), \tag{s1}$$

where, K is a material related proportionality constant, k is Boltzmann's constant and T is the temperature.

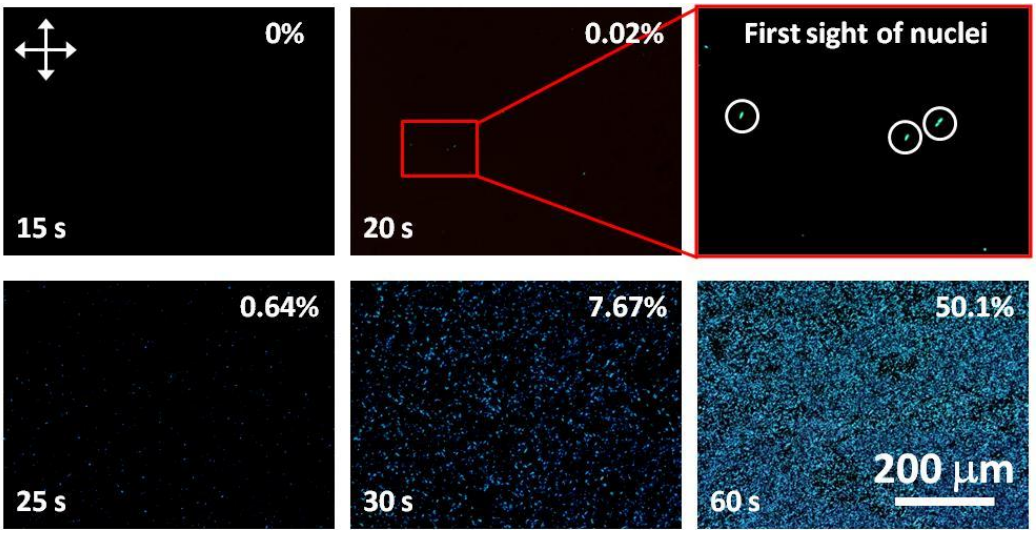

fig. S4. Polarized optical micrographs of MoO_x thin films (100 nm) at different annealing times. The duration of annealing is marked on the bottom left corner of the image and the estimated percentage of thin film conversion to crystalline phase is marked at the top right corner of each image. The nucleation starting time was taken as the first appearance of nuclei (the bright spots highlighted with white circles) in the polarized micrographs. In this case, the nucleation starting time was found to be ~20 s.

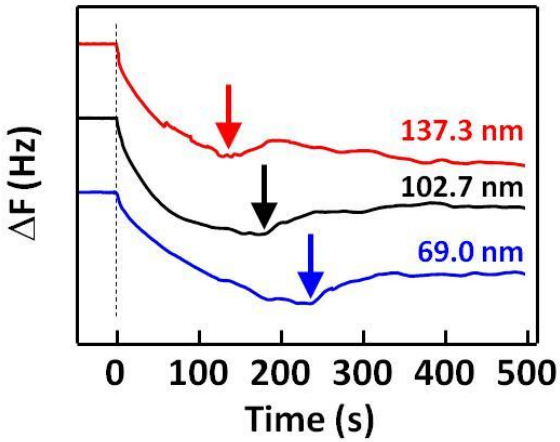

fig. S5. QCM-D measurements during solvent vapor annealing. The baseline (ΔF = 0) has been shifted for each plot for viewing clarity, hence the ordinate axis values have been removed. The measurement was conducted inside a custom-built environmental chamber which allows to monitor the mass uptake and loss by an amorphous TES ADT film cast on top of the quartz crystal sensor as it is exposed to a solvent vapor environment. The dashed line marks the point at which the solvent liquid is introduced into an open container in the environmental chamber and evaporates freely. The negative frequency shift seen in all cases indicates mass uptake by the amorphous films, namely solvent vapor molecules. As TES ADT begins to crystallize, the solvent taken up by the film is momentarily ejected by the growing crystalline phase, providing a clear bump in ΔF at the onset of nucleation of TES ADT crystals (see arrows). The onset of crystallization shifts to later times for thicker film (the thickness of the amorphous films is indicated).

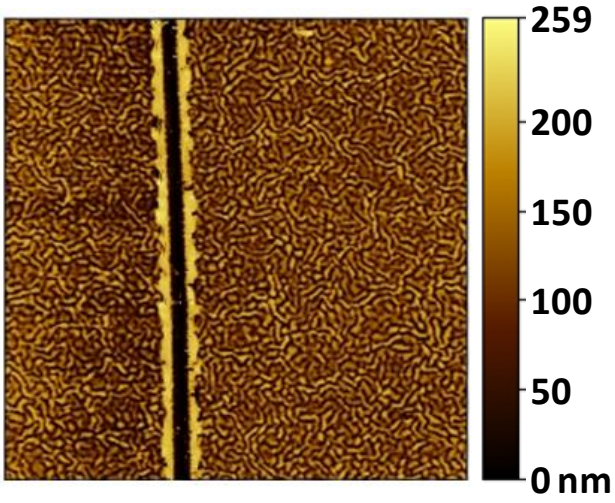

fig. S6. Atomic force microscopy topography image of a TES ADT film scratched with a needle. The size of the image is 80 μm × 80 μm.

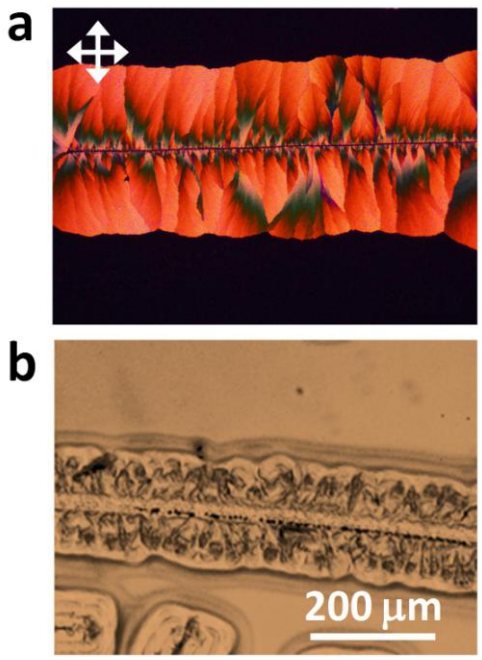

fig. S7. Optical micrographs of TES ADT and PCBM films crystallized using linear seeding.

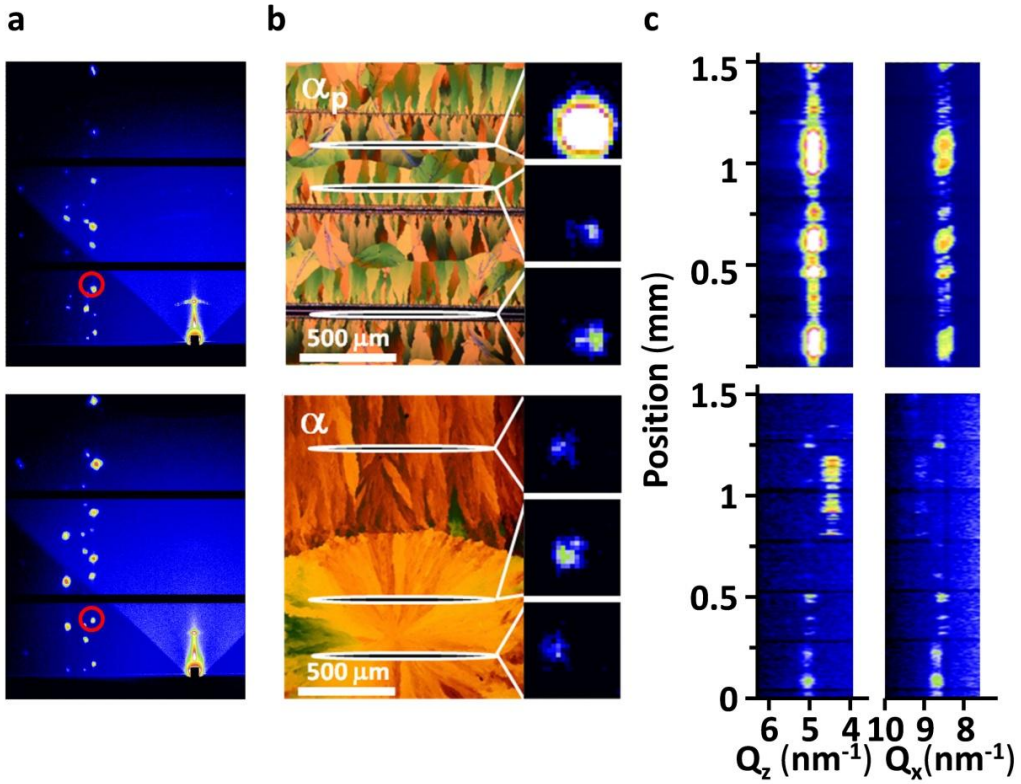

fig. S8. µGIWAXS images of the α_p and α phases. (A) Typical µGIWAXS image taken for the αp phase (top) and α phase (bottom), with the (011) diffraction marked in red circle. The V-shape imprint in the background results from the holder of the capillary for the micro-beam setup. b) Polarized optical micrograph of the two phases with µGIWAXS image of (011) at

marked positions. c) μGIWAXS mapping of (011) diffraction respect to the position in optical micrograph in b integrated in Q_x and Q_z axis.

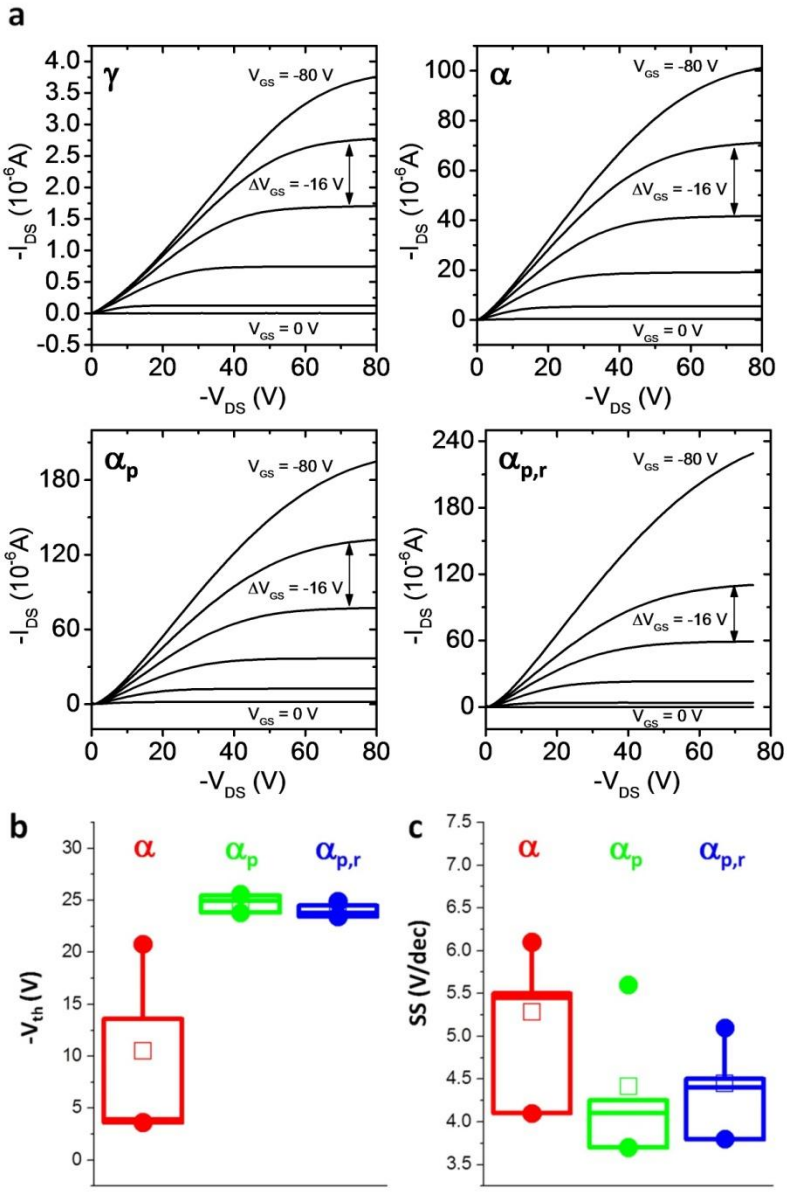

fig. S9. (A) Four typical OFET output characteristics of TES ADT thin film in each crystalline structure. (b,c) statistics of the threshold voltage (b) and sub-threshold swing (c) of the devices in a (Solid circles represent the maximum and minimum values, empty square represent the mean value, box represent the 20% to 75% of the values).

movie S1. Conventional crystallization of a TES ADT film proceeding stochastically and incoherently.

movie S2. Linear programmed crystallization of TES ADT proceeding simultaneously and coherently from horizontal seeding lines.

movie S3. Periodic dot array crystallization of TES ADT proceeding simultaneously and coherently from an array of imprinted seed dots.

movie S4. Square programmed crystallization of TES ADT proceeding simultaneously and coherently from horizontal and vertical seeding lines.

movie S5. Square and rectangular programmed crystallization of TES ADT proceeding simultaneously and coherently from horizontal and vertical seeding lines.